

Self-assembled in-plane Ge nanowires on rib-patterned Si (1 1 10) templatesLei Du,¹ Daniele Scopece,^{2,3} Gunther Springholz,⁴ Friedrich Schäffler,⁴ and Gang Chen^{1,4,*}¹*National Laboratory of Infrared Physics, Shanghai Institute of Technical Physics, Chinese Academy of Sciences, 500 Yutian Road, 200083 Shanghai, China*²*L-NESS and Department of Materials Science, Università di Milano-Bicocca, via R. Cozzi 53, 20126, Milano, Italy*³*Empa, the Swiss Federal Laboratories for Materials Science and Technology, Überlandstrasse 129, 8600 Dübendorf, Switzerland*⁴*Institute of Semiconductor and Solid State Physics, Johannes Kepler University, Altenberger Strasse 69, A4040 Linz, Austria*

(Received 14 April 2014; revised manuscript received 3 August 2014; published 20 August 2014)

Ge heteroepitaxy on Si (1 1 10) substrates induces the formation of prism-shaped in-plane nanowires bounded with {1 0 5} facets. In this work, in-plane nanowires were fabricated via the growth of Ge onto rib-patterned Si (1 1 10) templates oriented in the [55 $\bar{1}$] direction. Atomic force microscopy (AFM) reveals that a self-elongation of the nanowires occurs, resembling the phenomena observed on rib-patterned Si (0 0 1) templates, which indicates that this is a universal effect for nanowires grown on rib patterns. Finite-element simulations, performed with input from the latest *ab initio* calculations, reveal that the mechanism behind these phenomena is the minimization of the total energy density of the epilayer under rib-dominated geometry. Ge surface diffusion leads to a broadening of the Ge nanowires at the rib shoulder sites, which is proved to be an effective route to reduce the total energy density. Our results provide a straightforward solution for the realization of a single or a few Ge nanowires for potential device applications.

DOI: [10.1103/PhysRevB.90.075308](https://doi.org/10.1103/PhysRevB.90.075308)

PACS number(s): 68.35.bg, 62.23.Hj, 81.16.Dn, 68.37.Ps

I. INTRODUCTION

Due to their excellent properties and promising applications in electronics [1], optoelectronics [2], energy conversion and storage [3], thermoelectrics [4], and biomedical devices [5], semiconductor nanowires have been extensively studied in the last decade. Particularly, Ge-based nanowires have attracted substantial interest as an alternative route to meet the technical challenges rising from the miniaturization of complementary metal-oxide-semiconductor transistors [6,7], owing to their compatibility with the sophisticated Si-based semiconductor technology. So far, great success has been achieved regarding devices based on Ge and Ge/Si core/shell nanowires fabricated with the bottom-up vapor-liquid-solid (VLS) growth method [2,8], which have shown excellent device performance [9–11]. Nevertheless, the indispensable metallic catalyst nanoparticles involved in VLS methods [12], as well as the enormous efforts required for the transfer/arrangement of these vertically grown nanowires, have hampered further integration with microelectronics technology.

In this context, laterally aligned heteroepitaxial in-plane Ge nanowires on Si substrate have been regarded as an alternative solution [13]. Although this idea was suggested by Tersoff and Tromp two decades ago [13], its feasibility has been fully realized only recently with comprehensive studies on self-assembled Ge or SiGe nanowires on miscut Si (0 0 1) substrates [14,15], especially on the Si(1 1 10) surface [16–22], which is tilted off the (0 0 1) surface by 8.03° toward the [$\bar{1}$ 1 0] direction. The mechanism behind wire formation and their stability on Si(1 1 10) are attributed to the abnormal faceting of the wetting layer, which is driven by the low surface energy of their {1 0 5} side facets [22]. Similar nanostructures have also been achieved on the Si (0 0 1) surface, either by template patterning [23], or by extended thermal annealing of Ge hut clusters at low temperatures [24].

The application potential of lateral Ge nanowires for electronic [24] and spintronic devices has also been reported recently [25]. Nevertheless, there are still many issues to be addressed for the further development of nanowire devices. Since the Ge nanowires result from faceting of the Ge wetting layer on Si (1 1 10), the whole surface is covered by them. Their length is limited by interruptions and bifurcations [17,19], which make it difficult to define and to access a specified group of nanowires with reasonable uniformity in length, width, and straightness. In this work, we have applied the strategy of template patterning to achieve a self-alignment and self-elongation of such Ge nanowires on the top of ribs etched into the Si (1 1 10) substrates along the [55 $\bar{1}$] direction. Comprehensive total energy density studies via finite-element methods with input from *ab initio* calculations [26] were carried out to reveal the driving force behind the self-elongation. The underlying mechanism for these phenomena and the possible influence of Si/Ge intermixing and geometry are discussed on the basis of the experimental and simulation results.

II. METHODS

Si (1 1 10) substrates were cut into 9 × 9 mm² pieces. Smaller 200 × 200 μm² areas patterned with arrays of parallel ribs oriented along the [55 $\bar{1}$] direction were fabricated by electron beam lithography with a Leo Supra 35 field emission scanning electron microscope (FE-SEM) and subsequent reactive ion etching in an Oxford Plasmalab 80 reactor. The periodicity of the rib array is about 400 nm, the height of the ribs is about 50 nm, and their top width d is 150 nm. The bottom width equals the periodicity; i.e., the sidewalls of the ribs are inclined. The samples were prepared for solid source molecular beam epitaxy (MBE) by chemical precleaning with a final hydrofluoric acid treatment immediately before introduction into a Riber SIVA 45 MBE system. After an *in situ* thermal desorption step at 950 °C for 10 min, a 50-nm-thick Si buffer layer was deposited while ramping the substrate

*gchen@mail.sitp.ac.cn

temperature from 450 to 520 °C. Subsequently, 4.5 monolayers (ML) of Ge were deposited at 600 °C at a rate of 0.05 Å/s. After growth, the surface morphology was characterized *ex situ* with a Veeco Dimension 3100 atomic force microscope in the tapping mode. The Gwyddion[®] analysis package was used for image processing.

Modeling based on the experimentally observed geometry was performed by a finite-element method (FEM) analysis of the Ge nanowires with the commercial COMSOL Multiphysics[®] 3.5a package. In our idealized models, no intermixing was considered. Periodic boundary conditions were applied to simulate Ge nanowires of infinite length. To obtain the total energy density of the nanowires, first the strain field and the strain energy were calculated. Afterwards, the strain-dependent surface energy, as well as the edge energy [22] were determined by employing *ab initio* results for the Ge (1 0 5) [27], Ge (1 1 10) [28], and Ge (1 1 3) surfaces [29]. These results allow for a comparison of the total energy densities of different Ge nanowire configurations on the Si(1 1 10) ribs. For further discussion, an intermixing between the Ge nanowires and the Si template, as well as Ge surface diffusion on the rib sidewalls, was introduced to clarify the mechanism behind the experimentally observed broadening of the Ge nanowires at the rib shoulders.

III. RESULTS AND DISCUSSIONS

The surface morphology of a typical rib-patterned Si (1 1 10) template used in this work is shown in Fig. 1(a) as a three-dimensional (3D) AFM image corresponding to an area of $2 \times 2 \mu\text{m}^2$ and with a rib orientation aligned along $[55\bar{1}]$. The distance between neighboring ribs is 400 nm. The deposition of a Si buffer and 4.5 ML Ge leads to a sample surface decorated with faceted ripples for both the flat, i.e., unpatterned reference substrate [22], and the rib-patterned samples grown under identical conditions. Figure 1(b) is the derivative view of a $1 \times 1 \mu\text{m}^2$ AFM image of the flat (1 1 10) reference sample after Ge overgrowth. The two-dimensional (2D) fast Fourier transform (FFT; inset) gives an average ripple width of 12 ± 0.5 nm. The average height of the ripples is about 0.9 nm, and their length exceeds 100 nm.

Figures 2 and 3 show the surface morphology of the rib-patterned sample after 4.5 ML Ge deposition at 600 °C. Figure 2(a) and 2(b) shows the derivative and 3D views of a $2 \times 2 \mu\text{m}^2$ AFM image of the surface, respectively, showing that the surface morphology of the ribs is dominated by extended ripples along the direction defined by the $[55\bar{1}]$ oriented rib, while the remaining sidewall area of the sample is quite smooth. The length of the ripples is significantly increased up to $3 \mu\text{m}$, compared with those on the unpatterned reference sample [see Fig. 1(b)]. This is due to the self-alignment and coherent self-connection of the short ripple section into long and straight extended ripples [23], as can be well resolved as shown in the inset of Fig. 2(a). These elongated ripples will be referred to as nanowires in the following. Bifurcations and vacancies between the nanowires are hardly observed in this case. The average width of the nanowires at the middle of the rib top is 12 ± 0.5 nm, which is almost the same as on the flat surface. Thus, rib patterning of a Si (1 1 10) substrate significantly improves the uniformity

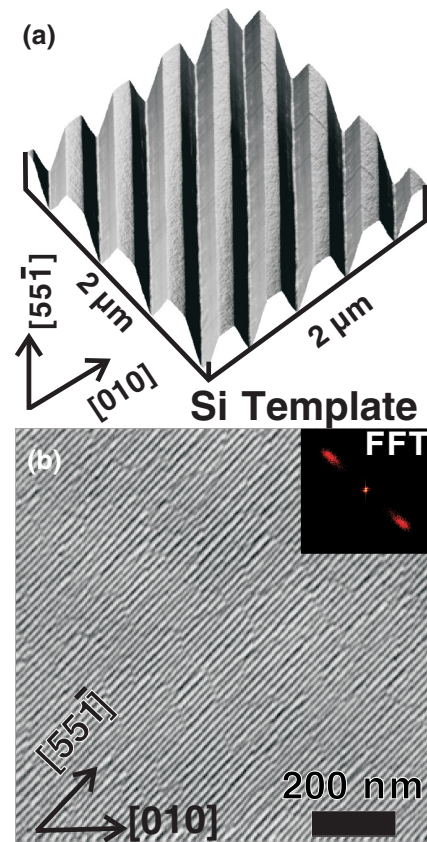


FIG. 1. (Color online) (a) 3D AFM image ($2 \times 2 \mu\text{m}^2$) of the initial rib-patterned Si (1 1 10) template with the ribs aligned along $[55\bar{1}]$; (b) derivative AFM image ($1 \times 1 \mu\text{m}^2$) of the unpatterned Si (1 1 10) substrate after the growth of 4.5 ML Ge at 600 °C.

of the self-assembled Ge nanowires, which resembles the phenomenon on the rib-patterned Si (0 0 1) template reported in our previous paper [23].

Figure 3(a) is a 3D view of an AFM image that highlights the perfectly aligned Ge nanowires on the top of a single rib of $1.4 \mu\text{m}$ length and 400 nm base width. The rib top is fully occupied by an array of seven nanowires covering the whole length. Its cross-sectional height profile is presented in Fig. 3(b), which is measured along the white line marked in Fig. 3(a). The width of the nanowires at the two rib shoulder sites is 15 to 18 nm, which is evidently broader than that for the inner nanowires, which have an average width of 12 nm. Such a localized broadening implies preferential accumulation of materials at the shoulder sites, as will be discussed below.

To shed light on the nature of the nanowire self-alignment and self-elongation, we have studied the energetics pathways for the nanowire configuration on the rib top. The total energy densities of nanowires in various model configurations were examined via FEM calculations, in which the strain energy, surface energy, as well as the edge energy term were taken into account [22]. Of course, direct experimental determination of the profile shape as well as of concentration of the Ge nanowires is always desirable. Nevertheless, in our work, the width of the prism-shaped Ge nanowire is merely about 12–15 nm, and thus their height is just about 0.84–1.05 nm, due to the fixed sidewall angle of 7.97°. Such a small cross section

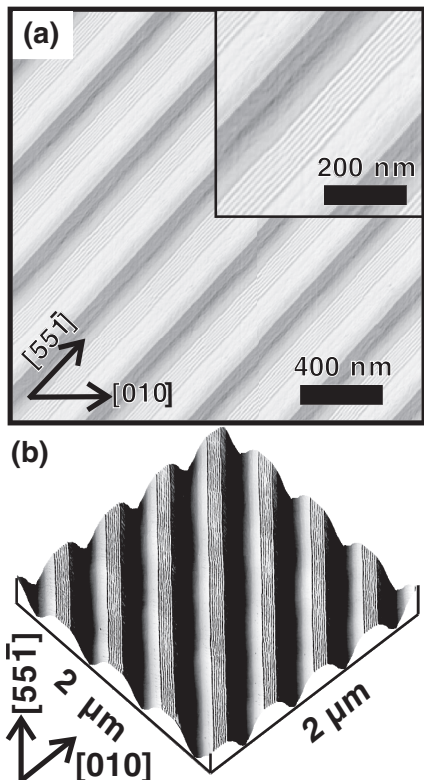


FIG. 2. (a) Derivative and (b) 3D AFM image of Ge nanowires sitting on ribs after the growth of 3.5 ML Ge at 650 °C. Image size: $2 \times 2 \mu\text{m}^2$.

makes observation very difficult even with transmission electron microscopy (TEM) combined with energy dispersive x-ray (EDX) analysis, although this technique is rather a powerful tool in the recent studies on SiGe colloidal core-shell nanocrystals [30] and nanowires [31]. Thus, in this paper,

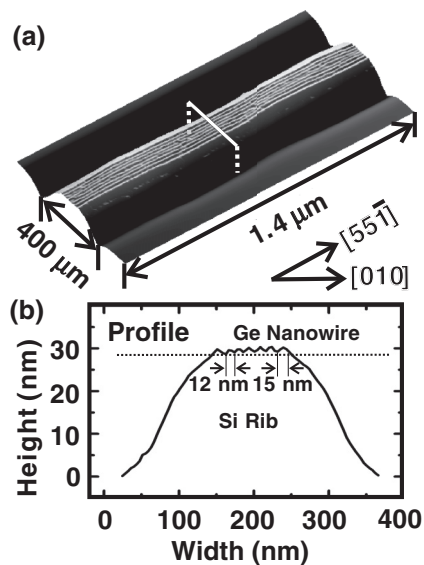


FIG. 3. (a) 3D AFM image showing the perfectly self-aligned and self-elongated Ge nanowires on a 1.4- μm -long section of a rib; (b) height profile measured across the white line marked in (a).

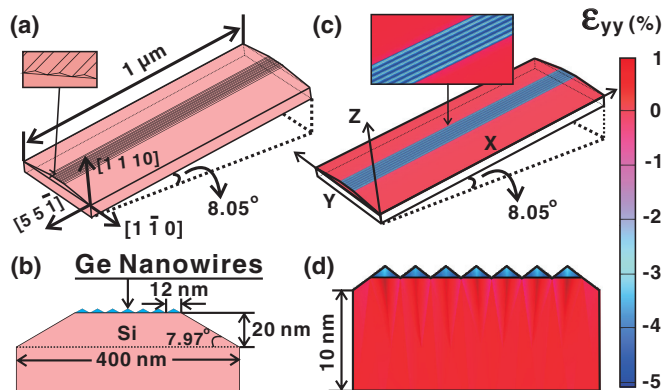


FIG. 4. (Color online) (a) 3D rendering of a typical model used for the FEM calculations, in which seven Ge nanowires are sitting on a $\{105\}$ faceted rib. The rib is tilted by 8.05° to the (001) surface to simulate the (110) oriented substrate; (b) schematic profile of the model; (c) and (d) 3D and cross-sectional view of the calculated strain distribution ϵ_{yy} over the Ge nanowires and the Si substrate underneath.

we generally follow the strategy that has been successfully applied in our previous paper [22]. There is no wetting layer considered in this case, since the nanowires are treated as a completely faceted wetting layer [22]. This is also due to the fact that at the growth temperature of 600 °C and a growth rate of 0.05 Å/s, Si/Ge intermixing at the interface is rather small [32–34], which leaves less than half a ML of Ge at the heterointerface below the nanowires [22]. In Fig. 4(a), a 3D rendering of a typical model used for the FEM calculations is presented, in which seven Ge nanowires with a length of $1 \mu\text{m}$ are sitting on a $\{105\}$ faceted rib to simulate the experimental observations shown in Figs. 2 and 3. In the calculation, infinitely long Ge nanowires on a Si rib are studied by using periodic boundary conditions. The whole slab, including the Si rib and the Ge nanowires, is tilted by 8.05° from the (001) surface to simulate the Si (110) oriented vicinal surface. Figure 4(b) shows a schematic profile of a simplified model, in which every Ge nanowire features a triangular cross section with a base width of 12 nm and a height of 0.84 nm. The broadening of the Ge nanowires at the rib shoulder is not taken into account for the moment. The whole model slab comprises a 100-nm-thick Si (001) base and a 20-nm-thick Si rib body. The rib section is 400 nm in bottom width and 84 nm in top width. In this idealized case, the two side walls of the Si rib are also fully decorated with one monolayer of Ge adatoms, and thus form continuous $\{105\}$ facets with the Ge nanowires sitting at the rib shoulder, as observed in this and previous papers [19]. As discussed later herein, the energetic contribution from the Si rib is not taken into consideration.

To obtain the total energy density of the nanowires, first the strain distribution and the elastic strain energy were calculated. Figure 4(c) and 4(d) shows the 3D and cross-sectional views of the calculated strain ϵ_{yy} over the Ge nanowires and the Si substrate underneath, respectively. It is clear that Ge nanowires have relaxed at the upper center region, while the base of the ripples is still significantly strained. Based on these results and with results from *ab*

initio calculations for Ge (1 0 5) [27], the strain energy and the strain-dependent surface energy are determined.

The total energy density ρ_{tot} is given by $\rho_{\text{tot}} = (E_{\text{str}} + E_{\text{surf}} + E_{\text{edge}})/V$, where E_{str} , E_{surf} , and E_{edge} stand for the elastic strain energy, surface energy, and edge energy terms, and V is the volume for the given single nanowire. The elastic strain energy density ρ_{str} and the surface energy density ρ_{surf} are also defined by $\rho_{\text{str}} = E_{\text{str}}/V$ and $\rho_{\text{surf}} = E_{\text{surf}}/S$, where S is the surface area of a given nanowire. In the case of noninterrupted nanowires, only the surface energy density of Ge (1 0 5) needs to be considered. Finally, the edge energy term E_{edge} is given by $E_{\text{edge}} = \rho_{\text{edge}} \times L$, where ρ_{edge} is the energy density of the top and two basal ripple facet intersections, and L is the length of the nanowire. In our calculation, a value of $\rho_{\text{edge}} = 3.7 \text{ eV/nm}$ is adopted as the edge energy density based on the quantitative analysis in our previous paper, and it is mainly attributed to the top edge rather than the basal intersections [22].

In Figure 5(a) to 5(c), the strain, surface, and total energy densities for the Ge nanowire sitting at either the middle or shoulder sites are shown as a function of the total number of nanowires on the rib. The strain energy of a nanowire sitting at the shoulder site is always lower than that of a wire at the middle site, due to the lack of a neighboring nanowire [Fig. 5(a)]. In the total energy balance, the elastic energy stored in the substrate is also evaluated, since the Si

rib itself can accommodate some deformation, particularly in the proximity of the rib shoulder. In a typical case with nine nanowires, the elastic energy for the Si rib is determined to be 825.89 eV in the FEM slab; i.e., each nanowire contributes 91.77 eV. Thus, the additional elastic energy density for one nanowire is of the order of $1.8 \times 10^{-2} \text{ eV/nm}^3$. Obviously, this is very small compared with the $\sim 1.5 \text{ eV/nm}^3$ average elastic energy density in a single nanowire. Thus, this effect is neglected in the further analysis. On the other hand, the surface energy density for the nanowire at a shoulder site is larger than that for one at a middle site [Fig. 5(b)]. Since the surface energy term dominates the total energy density for such small nanowire widths, the total energy density of a nanowire at a shoulder site is larger than that for the one at the middle site by 0.03 eV/nm^3 when nine nanowires are located at the rib top. This trend gets even more pronounced with an increasing number of nanowires on the rib top (not shown here).

In earlier papers, it has been observed that SiGe ripples/nanowires formed on Si (1 1 10) substrates are always hampered by misalignment and imperfection, including bifurcations, interruptions, etc. [17,18], which shorten the length of the nanowires far below $1 \mu\text{m}$, as shown in Fig. 1(b). On the other hand, as shown in Fig. 2, the length of a typical nanowire on the patterned rib top is increased up to $3 \mu\text{m}$, which implies that a self-connection mechanism is working to suppress the interruption or the discontinuity of the nanowires. To study this patterning-induced self-connection mechanism of the nanowires on the rib top, a vacancy that splits a continuous nanowire into two separate faceted sections is introduced into the nanowire model, as shown in Fig. 5(d). In this model, a narrow rib with three nanowires is considered. The vacancy is put in the middle of the central nanowire. The vacancy consists of one (0 0 1) and one (1 1 3) facet. The surface energy density of Ge (0 0 1) is about 6.1 eV/nm^2 [27]. Unlike the (0 0 1) facets, {1 1 3} facets usually can hardly be distinguished from the accumulated step-bunchings at the termination of a nanowire [19,35]. Lacking quantitative studies, it is difficult to take the Ge {1 1 3} facets into consideration in the FEM studies. However, with the recent progress in *ab initio* calculation [29], the key parameters of Ge {1 1 3} surface energies have become available. With these inputs (see table II in Ref. [29]) and the edge energy density fixed as 3.7 eV/nm , the corresponding strain energy density, surface energy density, and total energy density for the interrupted nanowire (both halves combined) are calculated to be 1.504 eV/nm^3 , 5.619 eV/nm^2 , and 15.127 eV/nm^3 , respectively, as represented by yellow diamonds in Fig. 5(a) to 5(c). All these values are slightly higher than those for one continuous nanowire by 0.05% (for strain energy density) to 0.3% (for total energy density), which indicates that the continuous nanowire is energetically more favorable than the interrupted one. In the case of longer nanowires, this discrepancy is reduced but still confirms this trend. This is because the vacancy introduces additional Ge {1 1 3} facets, the surface energy density of which is much higher than that of the Ge {1 0 5} facets under the given strain. Thus, the self-connection is driven by thermodynamic equilibrium, meaning that a further improvement of the geometrical perfection of the nanowires may be achieved by *in situ* annealing [24].

It should be noted that the vacancy is still a simplified model to simulate the imperfection of the nanowires. Bifurcation,

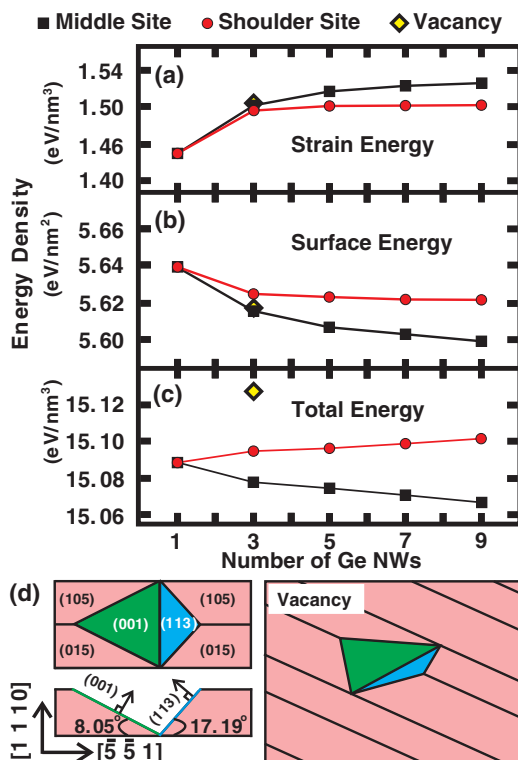


FIG. 5. (Color online) (a)–(c) Strain, surface, and total energy densities of a single Ge nanowire sitting at either middle (black squares) or shoulder site (red circles), as a function of the number of nanowires on the rib. The yellow diamond represents the corresponding values with a vacancy introduced in the nanowire array with the geometry shown in (d), representing the top, side, and 3D view of the scheme for a faceted vacancy introduced to simulate interrupted nanowires.

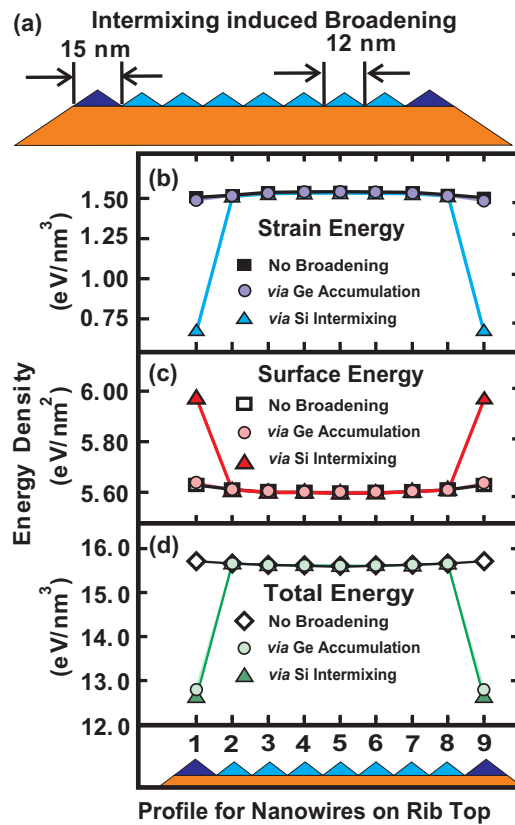


FIG. 6. (Color online) (a) Schematic model for the intermixing-induced broadening of the nanowires at the edge of the rib; (b)–(d) comparison of the strain, surface, and total energy densities of nine Ge nanowires sitting at different sites of the rib, with and without wire broadening at the shoulder sites through Si intermixing (triangles) or Ge accumulation (circles).

as a more common route to accommodate the misalignment of meeting nanowires, not only in the Si/Ge system, but also in a III-V system [36], has not yet been discussed here. The general formation mechanism for the bifurcation of self-assembled lateral nanowires will be addressed in a forthcoming publication.

So far in the FEM calculations, all modeled nanowires were of identical size. However, as shown in Fig. 3(b), the two nanowires sitting at the rib shoulder are slightly larger than the others. This indicates that accumulation of Ge adatoms at the shoulder and the rib sidewalls can play a role as an efficient diffusion channel [37]. To this end, we adopted a modified model, shown in Fig. 6(a), in which the broadening is attributed to accumulation of Ge adatoms that diffuse to the shoulder site from the Ge wetting layer on the corresponding rib sidewall [37]. The resulting Ge concentration in these nanowire is still assumed to be 100%; i.e., the only difference to the original model is the volume increase of the edge nanowires by 56% due to the increase of their width from 12 nm to 15 nm.

Si surface diffusion via the rib sidewall into the nanowires at a shoulder is a rather unlikely wire-broadening mechanism, because of the rather low growth temperature and the complete decoration of the rib sidewall surface with a Ge wetting layer [37]. Nevertheless, we also considered a model, in which the

broadening of the nanowires at shoulder sites is induced by Si incorporation. In this case, the Ge concentration in the shoulder nanowires is assumed to be reduced to 64% as estimated from the observed volumetric expansion. To accommodate the broadened nanowires, the width of the model rib was modified correspondingly.

The calculated strain, surface, and total energy density profiles for the three models of (i) uniform nanowires, as well as of broadened edge nanowires due to (ii) Ge accumulation, or (iii) Si incorporation and intermixing, are displayed in Fig. 6(b) to 6(d), respectively. For the uniform nanowires, where intermixing is absent, the strain energy density of the nanowires decreases monotonously from 1.532 eV/nm³ at the center site down to 1.508 eV/nm³ at the shoulder site, as indicated by the filled squares in Fig. 6(b). The corresponding surface energy density increases monotonously from 5.602 to 5.623 eV/nm² as shown in Fig. 6(c) by the hollow squares. In this case, the strain energy density decreases by 1.57% from the middle to the shoulder site, while the surface energy density increases only by 0.38%. The calculated total energy density profile follows a similar trend as the surface energy density, with an even smaller overall increase from middle to shoulder sites by 0.19%, as shown by the hollow diamonds in Fig. 6(d). Since the edge energy density is fixed at 3.7 eV/nm, it does not contribute to the variation in the total energy density profile.

If the broadening is induced by pure Ge accumulation [model (ii)], the strain energy density is 1.533 eV/nm³ at the middle site and 1.492 eV/nm³ at the shoulder sites. This difference of 2.67% suggests that Ge accumulation will indeed slightly enhance the reduction of the strain energy density at the shoulder sites, as indicated by the purple circles in Fig. 6(b). In this case, the surface energy density at the shoulder sites is only increased by 0.52% compared with the value at the middle site. On the other hand, introduction of local Si intermixing [model (iii)] drastically decreases the strain energy density at the shoulder site by 55.48%, as shown by the filled triangles in Fig. 6(c). This also leads to a 6.56% increase in surface energy density at the shoulder site compared with the middle site. Obviously, the broadening of the nanowire induced by both Ge accumulation and Si intermixing influences the strain energy density and the surface energy density at the shoulder sites. Nevertheless, the latter mechanism is far more pronounced than the former.

The total energy density for the uniform nanowire model without broadening, the Ge accumulation model, and the Si incorporation model is determined to be 15.760, 12.790, and 12.665 eV/nm³, respectively. This indicates that an increase of the nanowire volume at the rib shoulders by 56.25% will result in a significant decrease of the total energy density by 18.8% for Ge-accumulation-induced broadening, and by 19.6% for Si-diffusion-induced broadening. Thus, the nanowire broadening at the shoulders can significantly reduce the total energy density of the system. Both Ge accumulation and Si diffusion are effective routes for the broadening mechanism. Si diffusion is marginally more favorable than Ge accumulation by 0.8% of the total energy density reduction; nevertheless, its contribution to nanowire broadening at the rib shoulder is kinetically limited, as already discussed. On the other hand, the Ge wetting layer covering the rib sidewall can conveniently provide enough migrating Ge adatoms. Moreover, the *ab initio*

calculations of the Ge {1 0 5} surface have revealed that the potential fluctuations on this reconstructed surface are very small. Thus, the {1 0 5} faceted sidewall provides a fast and almost isotropic route for the diffusion of Ge adatoms [38]. These effects finally lead most likely to the accumulation of Ge within the nanowire at the rib shoulders, and the consequent minimization of the local total energy density.

IV. CONCLUSIONS

Heteroepitaxy of Ge onto rib-patterned Si (1 1 10) templates oriented along the $[5\bar{5}\bar{1}]$ direction leads to the formation of several-micrometer-long, perfectly aligned in-plane nanowires. Based on finite-element calculations, the minimization of the total energy density of the nanowires is found

to be the driving force behind the observed self-assembly, self-extension, and self-connection phenomena, leaving just a minor role to kinetic effects. The mechanism behind the broadening of the Ge nanowires at the rib shoulder sites is attributed to Ge accumulation there. Our results provide a straightforward solution for the investigation of single or a few Ge nanowires as well as for potential device applications.

ACKNOWLEDGMENTS

This work is supported by the Chinese Academy of Science (Hundred Talents Program), the Austrian Science Fund (SFB025-IRON), and the Austrian Research Promotion Agency (PLATON), Vienna. We also acknowledge Francesco Montalenti for fruitful discussions.

-
- [1] J. Salfi, I. G. Savelyev, M. Blumin, S. V. Nair, and H. E. Ruda, *Nat. Nanotechnol.* **5**, 737 (2010).
- [2] X. F. Duan, Y. Huang, R. Agarwal, and C. M. Lieber, *Nature* **421**, 241 (2003).
- [3] B. Tian, X. Zheng, T. J. Kempa, Y. Fang, N. Yu, G. Yu, J. Huang, and C. M. Lieber, *Nature* **449**, 885 (2007).
- [4] A. I. Hochbaum, R. K. Chen, R. D. Delgado, W. J. Liang, E. C. Garnett, M. Najarian, A. Majumdar, and P. D. Yang, *Nature* **451**, 163 (2008).
- [5] W. Kim, J. K. Ng, M. E. Kunitake, B. R. Conklin, and P. D. Yang, *J. Am. Chem. Soc.* **129**, 7228 (2007).
- [6] A. M. Morales and C. M. Lieber, *Science* **279**, 208 (1998).
- [7] S. Kodambaka, J. Tersoff, M. C. Reuter, and F. M. Ross, *Science* **316**, 729 (2007).
- [8] Y. Y. Wu and P. D. Yang, *Chem. Mater.* **12**, 605 (2000).
- [9] W. Lu, J. Xiang, B. P. Timko, Y. Wu, and C. M. Lieber, *Proc. Natl. Acad. Sci. USA* **102**, 10046 (2005).
- [10] J. Xiang, W. Lu, Y. J. Hu, Y. Wu, H. Yan, and C. M. Lieber, *Nature* **441**, 489 (2006).
- [11] C. K. Chan, X. F. Zhang, and Y. Cui, *Nano Lett.* **8**, 307 (2008).
- [12] J. E. Allen, E. R. Hemesath, D. E. Perea, J. L. Lensch-Falk, Z. Y. Li, F. Yin, M. H. Gass, P. Wang, A. L. Bleloch, R. E. Palmer, and L. J. Lauhon, *Nature Nanotech.* **3**, 168 (2008).
- [13] J. Tersoff and R. M. Tromp, *Phys. Rev. Lett.* **70**, 2782 (1993).
- [14] H. Omi and T. Ogino, *Appl. Phys. Lett.* **71**, 2163 (1997).
- [15] K. Ohmori, Y. L. Foo, S. Hong, J. G. Wen, J. E. Greene, and I. Petrov, *Nano Lett.* **5**, 369 (2005).
- [16] G. Chen, H. Lichtenberger, G. Bauer, W. Jantsch, and F. Schäffler, *Phys. Rev. B* **74**, 035302 (2006).
- [17] P. D. Szkutnik, A. Sgarlata, A. Balzarotti, N. Motta, A. Ronda, and I. Berbezier, *Phys. Rev. B* **75**, 033305 (2007).
- [18] I. Berbezier and A. Ronda, *Phys. Rev. B* **75**, 195407 (2007).
- [19] B. Sanduijav, D. Matei, G. Chen, and G. Springholz, *Phys. Rev. B* **80**, 125329 (2009).
- [20] L. Persichetti, A. Sgarlata, M. Fanfoni, and A. Balzarotti, *Phys. Rev. Lett.* **104**, 036104 (2010).
- [21] Z. Zhong, H. Gong, Y. Ma, Y. Fan, and Z. Jiang, *Nanoscale Res. Lett.* **6**, 322A (2011).
- [22] G. Chen, B. Sanduijav, D. Matei, G. Springholz, D. Scopece, M. J. Beck, F. Montalenti, and L. Miglio, *Phys. Rev. Lett.* **108**, 055503 (2012).
- [23] G. Chen, G. Springholz, W. Jantsch, and F. Schäffler, *Appl. Phys. Lett.* **99**, 043103 (2011).
- [24] J. J. Zhang, G. Katsaros, F. Montalenti, D. Scopece, R. O. Rezaev, C. Mickel, B. Rellinghaus, L. Miglio, S. De Franceschi, A. Rastelli, and O. G. Schmidt, *Phys. Rev. Lett.* **109**, 085502 (2012).
- [25] J. Pan, T. Zhou, Z. Jiang, and Z. Zhong, *Appl. Phys. Lett.* **102**, 183108 (2013).
- [26] F. Montalenti, D. Scopece, and L. Miglio, *C. R. Phys.* **14**, 542 (2013).
- [27] S. Cereda, F. Montalenti, and L. Miglio, *Surf. Sci.* **591**, 23 (2005); D. C. Migas, S. Cereda, F. Montalenti, and L. Miglio, *ibid.* **556**, 121 (2004).
- [28] D. Scopece, F. Montalenti, and M. J. Beck, *Phys. Rev. B* **85**, 085312 (2012).
- [29] D. Scopece and M. J. Beck, *Phys. Rev. B* **87**, 155310 (2013).
- [30] F. Erogbogbo, T. Liu, N. Ramadurai, P. Tuccarione, L. Lai, M. T. Swihart, and P. N. Prasad, *ACS Nano* **5**, 7950 (2011).
- [31] B. Eisenhawer, V. Sivakov, A. Berger, and S. Christiansen, *Nanotechnology* **22**, 305604 (2011).
- [32] A. A. Baski, S. C. Erwin, and L. J. Whitman, *Surf. Sci.* **392**, 69 (1997).
- [33] G. Capellini, M. De Seta, and F. Evangelisti, *Appl. Phys. Lett.* **78**, 303 (2001).
- [34] O. G. Schmidt, U. Denker, S. Christiansen, and F. Ernst, *Appl. Phys. Lett.* **81**, 2614 (2002); U. Denker, H. Sigg, and O. G. Schmidt, *Appl. Surf. Sci.* **224**, 127 (2004).
- [35] B. Sanduijav, D. Scopece, D. Matei, G. Chen, F. Schäffler, L. Miglio, and G. Springholz, *Phys. Rev. Lett.* **109**, 025505 (2012).
- [36] H. Wen, Z. M. Wang, and G. J. Salamo, *Appl. Phys. Lett.* **84**, 1756 (2004).
- [37] U. Denker, M. Stoffel, and O. G. Schmidt, *Phys. Rev. Lett.* **90**, 196102 (2003).
- [38] F. Montalenti, D. B. Migas, F. Gamba, and L. Miglio, *Phys. Rev. B* **70**, 245315 (2004).